

# Study of slope integral extension mode decomposition method for bearing-nonlinear vibration signal

Yuanjun Dai<sup>1</sup>, Weiqiang Huang<sup>2</sup>, Kunju Shi<sup>3</sup>

School of Mechanical College, Shanghai DianJi University, Shanghai, 201306, China

<sup>3</sup>Corresponding author

**E-mail:** <sup>1</sup>24354267@qq.com, <sup>2</sup>hwq1261712081@163.com, <sup>3</sup>shikunjv@sina.cn

Received 1 February 2023; accepted 18 April 2023; published online 22 July 2023

DOI <https://doi.org/10.21595/jve.2023.23197>



Copyright © 2023 Yuanjun Dai, et al. This is an open access article distributed under the Creative Commons Attribution License, which permits unrestricted use, distribution, and reproduction in any medium, provided the original work is properly cited.

**Abstract.** This study aims to solve the problem of extreme point ambiguity caused by energy instability at the signal end. Thus, an adaptive nonlinear signal decomposition method based on motion energy accumulation division is proposed, namely slope integral extension mode decomposition (SIEMD). The proposed method considers the fluctuation rate and vibration energy between the peaks of the waveform as its scale. Firstly, the comprehensive index is defined to adaptively select the ideal interval, and the extension characteristics of the waveform signal are obtained. Secondly, the energy of the waveform interval is iterated. Hence, the optimal extension waveform is fitted by combining the edge position information of the curve. The experimental part verifies that the method can extract 92 % of the fault information, and verifies that the proposed method overcomes the limitation of the previous one-dimensional signal waveform dimension. Moreover, from the perspective of signal energy, it eliminates the false information of the intrinsic modal function (IMF) components, more suitable for the randomness of the signal, thereby providing a new way for fault feature extraction.

**Keywords:** empirical mode decomposition, end effect, slope integral waveform matching, nonlinear signal decomposition.

## 1. Introduction

The internal structure of mechanical equipment is becoming increasingly complex. The generated nonlinear and non-stationary signals have higher requirements for the decomposition method [1, 2]. Hilbert-Huang transform (HHT) is a nonlinear and non-stationary signal analysis method proposed by Huang et al. [3] in 1998, which includes empirical mode decomposition (EMD) and Hilbert spectrum analysis. This method has been widely used in fault diagnosis [4], transformer's winding faults [5], power prediction [6, 7], and several other fields [8-10]. However, the EMD has issues with endpoint effect [11] and modal confusion [12, 13], which results in false components and makes it difficult to extract fault frequency.

To mitigate the endpoint effect, many scholars have suggested a series of improved methods such as polynomial extension [14, 15], extreme point symmetry extension [16], slope matching waveform extension [17, 18], prediction extension based on correlation vector machine [19], and prediction extension based on HLS-SVDR (Homotopy Least Squares-Support Vector Double Regression) [20]. The polynomial and symmetric extension method of extreme points is based on the characteristics of the EMD to extract the extreme points and form the envelope curve. According to certain polynomial extension methods [14, 15], the extreme points at the end are constructed and extended. The calculation involved in this method is straightforward. The extreme points of the extension area are obtained by integrating the data near the end points. For non-stationary signals, it is assumed that a portion of the extreme information alone cannot effectively suppress the end effect. The slope matching waveform extension is based on the slope of the waveform at the end to match the internal optimal interval of the signal. The waveform is copied to the end to suppress the end effect. However, this method limits the development trend of the extension waveform. It is unsuitable for signals with large oscillation amplitude and high sampling

frequency. The predictive extension method can achieve good extension effect. However, the calculation is complex, the operation efficiency is low, and a significant amount of data training is needed to achieve high accuracy.

The method proposed in our study uses features of the signal, such as slope and extreme value, to match the original signal waveform. The slope indicates the change in the trend of signal waveform. The change of waveform area reflects the change of waveform shape and energy. The SIEMD method proposed in this study synthesizes the slope and integral energy between the extreme points. It determines the extreme points using the slope of the optimal matching waveform and extends the waveform on both sides of the original signal using the least squares-polynomial. The waveform area is used as the basis for the continuation of the waveform.

The remaining structure of the paper is organized as follows. Section 2 describes the EMD algorithm and analyzes the causes of the endpoint effect. Section 3 analyzes the relationship between slope integral and waveform. Section 4 introduces the SIEMD algorithm. Sections 5 and 6 discuss simulation and engineering verification. Section 7 provides conclusions.

## 2. The EMD and endpoint effect analysis

### 2.1. EMD

The EMD can adaptively decompose the signal  $x(t)$  into a series of AM-FM (Amplitude & Frequency Modulated) signals, including  $n$  IMF components and a residual component  $r_n(t)$ [21]. The signal can then be written as:

$$x(t) = \sum_{i=1}^n IMF_i(t) + r_n(t). \tag{1}$$

And the EMD algorithm can be seen in Table 1.

**Table 1.** Empirical mode decomposition

Algorithm 1 Empirical Mode Decomposition
Input: input signal $r_1(t) = x(t)$ , iteration times $i = 1$
Output: IMF components $\{IMF_i(t)\}_{i=1}^n$ , a residual component $r_n(t)$
1: While $r_i(t)$ does not satisfy a constant or monotonic function do
2: $max_i(t) \leftarrow findpeaks(r_i(t)), min_i(t) \leftarrow findpeaks(-r_i(t))$
3: $s1_i(t) \leftarrow spline(max_i(t)), s2_i(t) \leftarrow spline(min_i(t))$
4: $m_i(t) \leftarrow (s1_i(t) + s2_i(t))/2$
5: $h_i(t) \leftarrow r_i(t) - m_i(t)$
6: While $mean(h_i) \neq 0$ do
7: $max_i(t) \leftarrow findpeaks(h_i(t)), min_i(t) \leftarrow findpeaks(-h_i(t))$
8: $s1_i(t) \leftarrow spline(max_i(t)), s2_i(t) \leftarrow spline(min_i(t))$
9: $m_i(t) \leftarrow (s1_i(t) + s2_i(t))/2$
10: $h_i(t) \leftarrow r_i(t) - m_i(t)$
11: End
12: $IMF_i(t) \leftarrow h_i(t)$
13: $r_{i+1}(t) \leftarrow r_i(t) - h_i(t)$
14: $i \leftarrow i + 1$
15: End

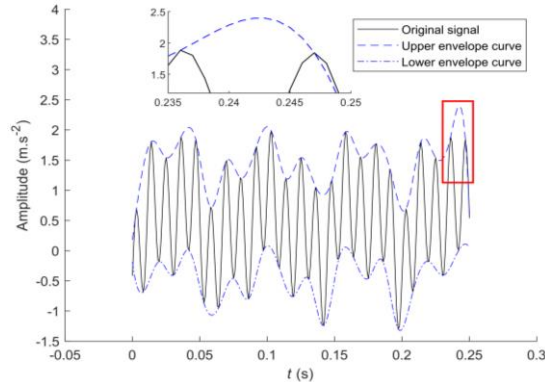
### 2.2. Endpoint effect analysis

As the endpoint of a data sequence may not be the extreme point, the cubic spline interpolation of the extreme point set will lead to a sharp change in the envelope curve at the endpoint. With

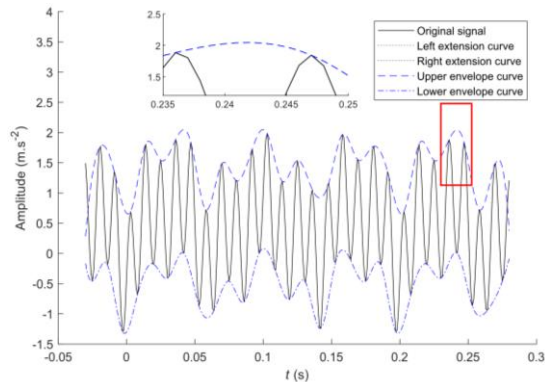
the increase of decomposition times, this phenomenon can gradually pollute the residual signal [22, 23].

Fig. 1 shows the fitting of the upper and lower envelopes of the data sequence directly using cubic spline interpolation. The simulation signal is obtained by:

$$x(t) = \sin(90\pi t) + \cos(1 + \cos(20\pi t) * \cos(50\pi t)). \quad (2)$$



**Fig. 1.** Traditional EMD decomposition without extension



**Fig. 2.** The EMD decomposition after extension

The solid line in Fig. 1 is the original signal given by Eq. (2) in the interval [0, 0.25] s. The dashed and dash-dotted lines are the upper and lower envelopes of the original signal, respectively. Fig. 1 shows that the envelope curve has a large oscillation at the right end of the signal. The envelope line and data sequence intersect in the local amplification diagram in Fig. 1, which cannot contain all the data. Hence, it cannot ensure the correct decomposition of the signal. The standard deviation of the upper envelope without extension is 0.4022 and the peak index is 1.5517.

To prevent the occurrence of this phenomenon, it is necessary to extend the waveform at both ends of the signal and increase the length of the waveform to suppress the endpoint effect [24].

Fig. 2 extends the signal length to [-0.03, 0.28] s, where the dotted line is the signal extended on both sides. The standard deviation of the envelope is 0.3959 and the peak index is 1.3828. Compared to the local amplification diagram of Figs. 1-2, the waveform after extension is smoother. It can reduce the possibility of sharp changes at the end. Therefore, the signal extension significantly inhibits the endpoint effect. There is no irregular oscillation of the fitting curve, and the data are not included.

In summary, a signal cannot be accurately decomposed by relying only on its extreme points to suppress the endpoint effect. It is necessary to extend the two ends of the signal and combine

them with the change trend of the original signal waveform. One maximum and one minimum values are added at both ends of the signal [25]. The endpoint effect is moved outward to reduce the decomposition error of the original signal.

### 3. Relationship between slope integral and waveform

The peak solution [26, 27] is the limit state that reflects the amplitude fluctuation within the local time-length. It extracts the adjacent maximum (minimum) of the signal waveform to form a peak decomposition diagram and is effectively applied in the time-frequency domain of nonlinear signals. The adjacent maximum (minimum) is of great significance for fault feature extraction.

As shown in Fig. 3, points  $A$  and  $B$  are two adjacent maximum points on a sinusoidal signal. The slope of line  $l_{AB}$  is zero. When point  $C$  on the point line is a point on the signal, the slope of line  $l_{AC}$  is not zero. When the signal waveform changes suddenly, the slope between adjacent maximum points changes [28]. That is, the slope is an important indicator of waveform change trend. Fig. 3 shows that although the signal  $y_2(t)$  and  $y_3(t)$  intersect at the maximum point  $C$ , the signal waveforms and amplitudes of the two are different.  $E_{y_2}$  denotes the integral of the line  $l_{AC}$  and signal  $y_2(t)$  in the range of  $[t_C, t_A]$ , that is, the vibration energy in the interval.  $E_{y_3}$  denotes the integral of the line  $l_{AC}$  and signal  $y_3(t)$  in the range of  $[t_C, t_A]$ . The randomness of the signal is visible in Fig.3. It implies that  $E_{y_2} \neq E_{y_3}$ . Therefore, the vibration energy reflects the amplitude and waveform shape. Through the above analysis, it is evident that slope and vibration energy are important indices of waveform, and the key references for waveform extension.

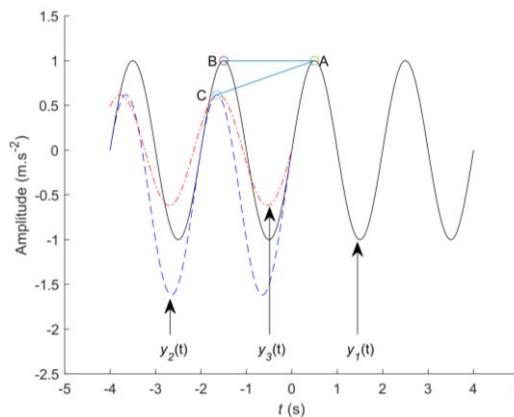


Fig. 3. Relationship between vibration energy and slope

### 4. SIEMD algorithm design

To overcome the above mentioned shortcomings and improve the matching degree of the extended signal, the SIEMD method is proposed in this study. This method is based on the segmentation baseline and motion energy in the signal extreme point interval. It matches the interval and extracts the extension characteristics. Finally, it fits the optimal extension curve using motion energy as the iterative termination condition. Assuming that the first extreme value of the signal is the maximum value, the implementation steps are as follows.

Find the extreme value: The extreme points of the original signal are calculated. The set of local maximum points is  $E_{\max}$ , and the corresponding time set is  $t_{\max}$ . The set of local minimum points is  $E_{\min}$ , and the corresponding time set is  $t_{\min}$ .

Seek slope and motion energy of the extreme point interval. The slope  $k_1$  (Eq. (3)) and segmentation baseline  $y_1$  (Eq. (4)) of points  $(t_{\max}^1, E_{\max}^1)$  and  $(t_{\max}^2, E_{\max}^2)$  are calculated. The function of fitting curve  $E_{\max}^1 E_{\min}^1 E_{\max}^2$  with least squares polynomial is  $s_1$ . The motion energy

$S_1$  surrounded by the segmentation baseline  $y_1$  and curve  $s_1$  is calculated (Eq. (5)). The order  $m_1$  needs to be determined for least squares polynomial fitting. The symbol  $len$  represents the length of set  $E_{max}$ . To ensure the fitting accuracy,  $m_1 = 6$ .

The slope calculation equation is as follows:

$$\begin{cases} k_1 = \frac{E_{max}^2 - E_{max}^1}{t_{max}^2 - t_{max}^1}, \\ k_2 = \frac{E_{max}^3 - E_{max}^2}{t_{max}^3 - t_{max}^2}, \\ \vdots \\ k_{end-1} = \frac{E_{max}^{len} - E_{max}^{len-1}}{t_{max}^{len} - t_{max}^{len-1}}. \end{cases} \quad (3)$$

The calculation equation of segmentation baseline is as follows:

$$\begin{cases} y_1 = k_1(t - t_{max}^1) + E_{max}^1, \\ y_2 = k_2(t - t_{max}^2) + E_{max}^2, \\ \vdots \\ y_{len-1} = k_{len-1}(t - t_{max}^{len-1}) + E_{max}^{len-1}. \end{cases} \quad (4)$$

The motion energy calculation equation is as follows:

$$\begin{cases} S_0 = \int_{t_{max}^0}^{t_{max}^1} (y_0 - s_0) dt, \\ S_1 = \int_{t_{max}^1}^{t_{max}^2} (y_1 - s_1) dt, \\ \vdots \\ S_{len-1} = \int_{t_{max}^{len-1}}^{t_{max}^{len}} (y_{len-1} - s_{len-1}) dt. \end{cases} \quad (5)$$

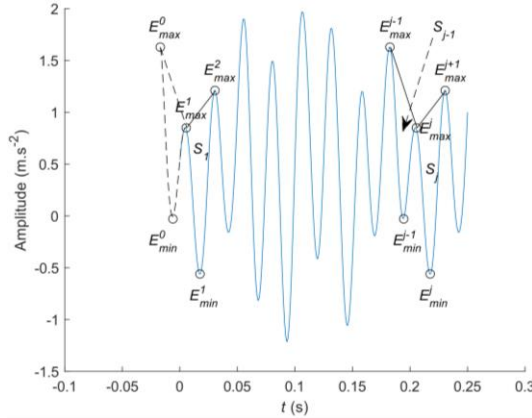
Select the optimal matching curve  $s_j$  with  $s_1$  according to the comprehensive index  $I_j$ . The slope set is  $k = [k_1, k_2, \dots, k_{len-1}]$ , and the motion energy set is  $S = [S_1, S_2, \dots, S_{len-1}]$ . The comprehensive index is  $I_i = |S_1 - S_i| + |k_1 - k_i| (1 < j \leq len - 1)$ . Considering the sampling frequency,  $|S_1 - S_i|$  and  $|k_1 - k_i|$  are not in one order of magnitude. Therefore, the comprehensive indicators are improved as:  $I_i = A * |S_1 - S_i| + B * |k_1 - k_i|$ . In the equation,  $A$  and  $B$  represent the proportion of slope and integral differences, respectively. They can be adjusted according to practical application scenarios. In this study,  $A = 10^3$ ,  $B = 10^{-2}$ . The set  $I = [I_1, I_2, \dots, I_{len-1}]$  is obtained by the slope set and the motion energy set. The interval corresponding to the minimum comprehensive index  $I_j (1 < j \leq len - 1)$  is selected. Subsequently, the curve  $s_j$  of the interval is determined to be the most similar to the curve  $s_1$ .

Extract the extension information. According to the step 3, the values of slope  $k_{j-1}$  and motion energy  $S_{j-1}$  from  $E_{max}^{j-1}$  to  $E_{max}^j$  are calculated, the data length of the interval  $n$  is counted, and position relationship  $p_{j-1}$  between the minimum point  $t_{min}^{j-1}$  and maximum point  $t_{max}^j$  in the interval is stored.

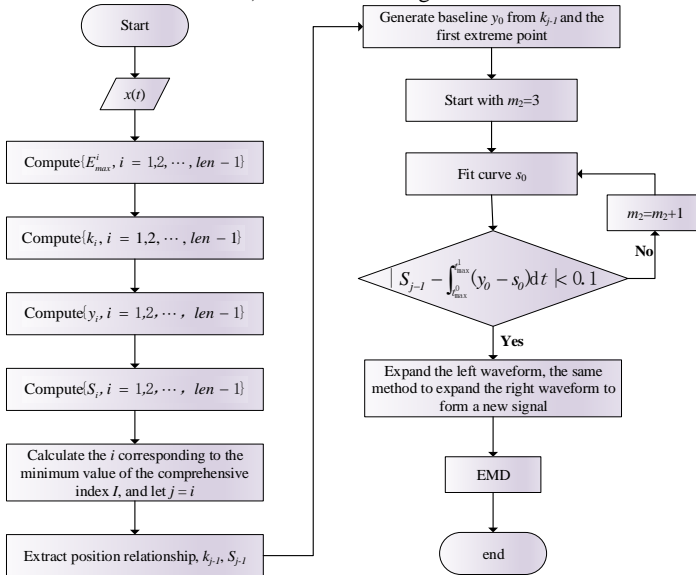
Extension waveform. Segmentation baseline  $y_0$  is based on the values of  $k_{j-1}$ ,  $t_{max}^1$  and  $E_{max}^1$ . Maximum  $E_{max}^0$  and minimum  $E_{min}^0$  of extension interval are calculated according to the data number  $n$ , the baseline  $y_0$  and position relationship  $p_{j-1}$ . The least square polynomial fitting

curve  $s_0$  is obtained by synthesizing the data of extreme points and endpoints of extension. The order of the least square method is  $m_2 = 3$ . The motion energy  $S_0$  is calculated (Eq. (5)). When the termination condition  $A * |S_0 - S_{j-1}| < 0.1$  is satisfied, the output curve  $s_0$  is the left extension waveform. Otherwise, let  $m_2 = m_2 + 1$ , repeat  $s_0$  and compare the size of  $A * |S_0 - S_{j-1}|$  and 0.1 in each case until the termination condition is satisfied.

The left extension is completed. The extension process is shown in Fig. 4(a). If the first extreme value is the minimum value, it is similar to the above mentioned method. Thus, the right endpoint extension curve can also be derived. The new signal is obtained and IMFs are obtained by the EMD decomposition.



a) The SIEMD diagram



b) The SIEMD flow chart

Fig. 4. Slope integral extension diagram

## 5. Simulated signal analysis

To verify the feasibility of the SIEMD method proposed in this study, the simulation signal is decomposed and compared with the EMD and the mirror extension of the EMD. The simulation signal expressions used are as follows:

$$\begin{cases} x_1(t) = \sin(800\pi t + 0.5\sin(50\pi t))(1 + 0.5\cos(50\pi t)), \\ x_2(t) = \sin(200\pi t), \\ x_3(t) = \sin(40\pi t), \\ x(t) = x_1(t) + x_2(t) + x_3(t). \end{cases} \quad (6)$$

The sampling frequency is 1000 Hz, the variable range is  $t \in [0, 0.5]$  s, and the original signal waveforms are shown in Fig. 5.

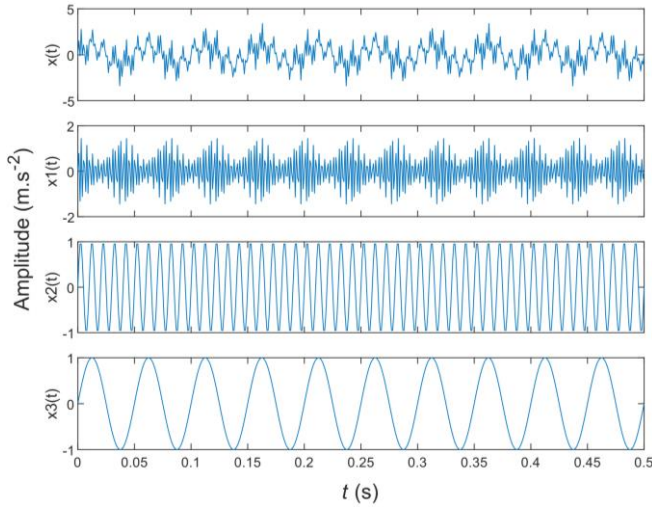


Fig. 5. Original signal and its component signals

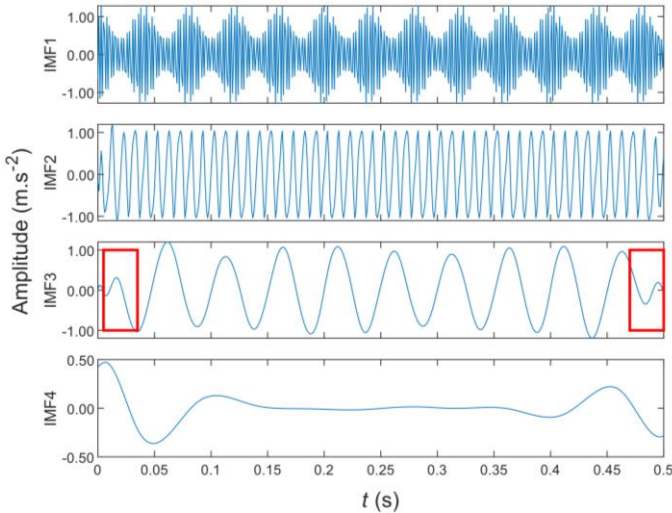


Fig. 6. The EMD decomposition without endpoint processing

Figs. 6-8 are the signals of Eq. (6) obtained by non-extension EMD, mirror extension EMD, and SIEMD, respectively. Due to the decomposition of more components, the first four are selected here for display. Compared with the intermediate waveform of IMF3 component, there is a large amplitude error in Fig. 6 and Fig. 7, and there is a serious endpoint effect. The waveform at the red mark in Fig. 8 is more consistent with the whole, which greatly suppresses the endpoint effect. Compared with the IMF4 component, the amplitude obtained by the SIEMD method is



smaller than other methods, showing a smaller decomposition error. Thus, the mirror extension method cannot effectively suppress the endpoint effect in Eq. (7):

$$E = x(t) - (IMF_1(t) + IMF_2(t) + IMF_3(t)). \quad (7)$$

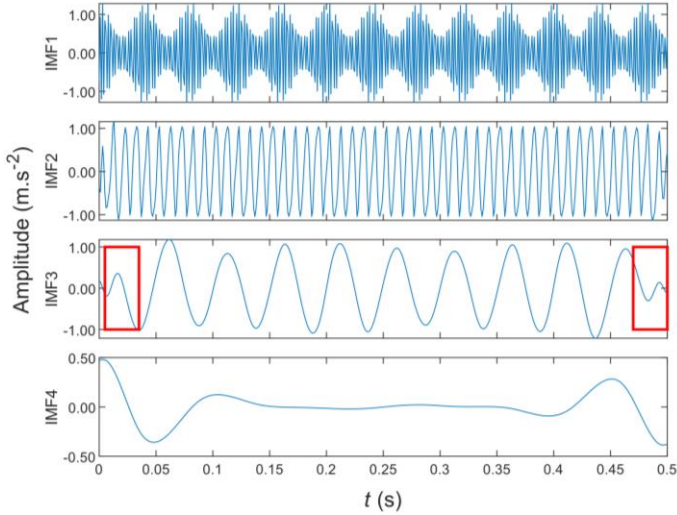


**Fig. 7.** Mirror extension of the EMD decomposition

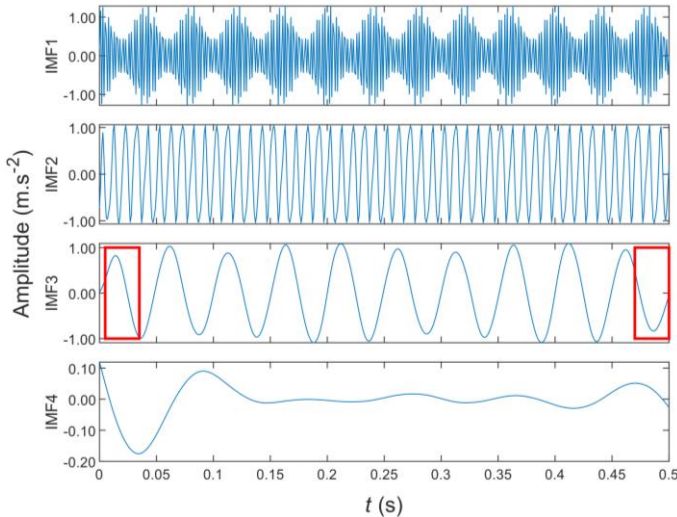


**Fig. 8.** The SIEMD decomposition

Fig. 9 is based on Eq. (7) to calculate the error between the original signal  $x(t)$  and the first three components obtained after the EMD decomposition. Fig. 9 shows that compared with the EMD decomposition and the mirror EMD decomposition, the SIEMD decomposition error is negligible. There are no significant oscillations at both ends. It shows that the SIEM significantly suppresses the endpoint effect.

The following two indices are used to evaluate the effect of the endpoint-effect processing method.

1) The correlation coefficient  $\rho$  between each component after the EMD decomposition and corresponding component of the original signal are calculated to evaluate the effect of endpoint



suppression:

$$\rho_i(x_i(t), IMF_i(t)) = \frac{\text{cov}(x_i(t), IMF_i(t))}{\sqrt{\sigma(x_i(t))} \sqrt{\sigma(IMF_i(t))}} \quad (8)$$

where  $\text{cov}(\cdot)$ ,  $\sigma(\cdot)$ ,  $IMF_i(t)$  and  $x_i(t)$  represent the covariance, the variance, the  $i$ th IMF component of the original signal after the EMD decomposition, and the  $i$ th corresponding component of the original signal, respectively. A value of  $\rho_i(x_i(t), IMF_i(t))$  closer to 1 indicates better endpoint suppression.

2) The average relative error between components after the EMD decomposition and corresponding components of the original signal are calculated:

$$\text{error}_{IMF_i} = \frac{\text{sqrt}\left(\sum_{k=1}^N [x_i(k) - IMF_i(k)]^2\right)}{N} \quad (9)$$

where  $N$ ,  $IMF_i(k)$ , and  $x_i(k)$  represent the number of signal acquisition, and  $k$ th data in the  $i$ th corresponding component of the original signal, respectively. The closer is  $\text{error}_{IMF_i}$  to 0, the smaller is the error between the decomposed and original signals.

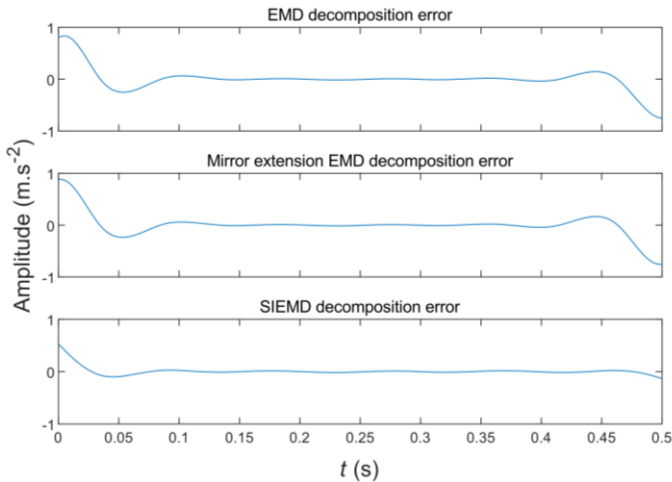


Fig. 9. The EMD, mirror EMD, and SIEMD decomposition error

According to Eqs. (5-6), the evaluation indexes of non-extension, mirror extension, and SIEMD are calculated. The results are listed in Table 2.

Table 2. Evaluation index values of non-extension, mirror extension, and SIEMD

	Non-extension	Mirror extension	Non-extension
$\rho_1(x_1(t), IMF_1(t))$	0.9713	0.9711	0.9720
$\rho_2(x_2(t), IMF_2(t))$	0.9465	0.9451	0.9505
$\rho_3(x_3(t), IMF_3(t))$	0.9475	0.9467	0.9915
$\text{error}_{IMF_1}$	0.0082	0.0082	0.0081
$\text{error}_{IMF_2}$	0.0106	0.0107	0.0102
$\text{error}_{IMF_3}$	0.0102	0.0102	0.0041

By the SIEMD method, the values of  $\rho_1(x_1(t), IMF_1(t))$ ,  $\rho_2(x_2(t), IMF_2(t))$  and  $\rho_3(x_3(t), IMF_3(t))$  are 0.9720, 0.9505 and 0.9915, respectively, which are closer to 1. The results

presented in Table 1 reveal that the correlation coefficient of the SIEMD method is greater than the EMD decomposition of non-extension and mirror extension. The average relative error of the EMD decomposition by the SIEMD method is less than that of the EMD decomposition without extension and mirror extension. By the SIEMD method, the value of  $error\_IMF_i$  is closer to 0. This indicates the effectiveness and feasibility of the SIEMD method.

## 6. Actual signal analysis

To further verify the effectiveness of the extension method, a nonlinear and non-stationary bearing fault signal is analyzed. The fault signal is collected from a test rig containing faulty bearings. The test bench shown in Fig. 10(a) is composed of motor, drive shaft, test rolling bearing and signal acquisition system. A crack with a width of about 0.2 mm is cut at the inner ring (see Fig. 10(b)) of the bearing by wire cut electrical discharge machining. The motor speed is 1940 r/min, and the theoretical bearing inner ring fault frequency is 159.96 Hz. The fault signal is shown in Fig. 11.

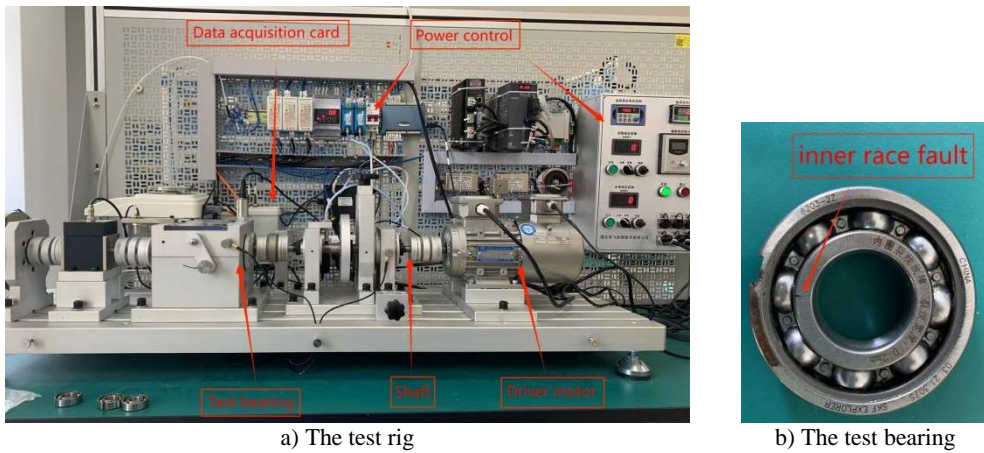


Fig. 10. Fault signal acquisition equipment

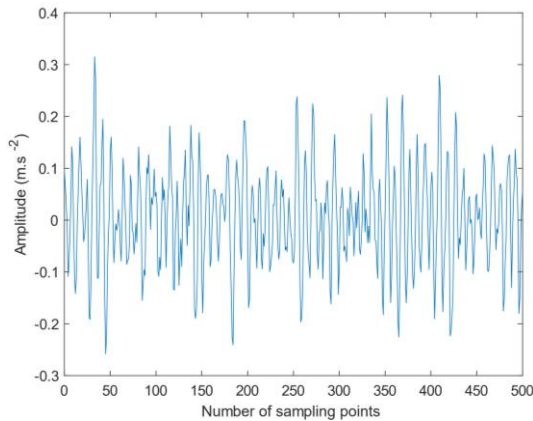
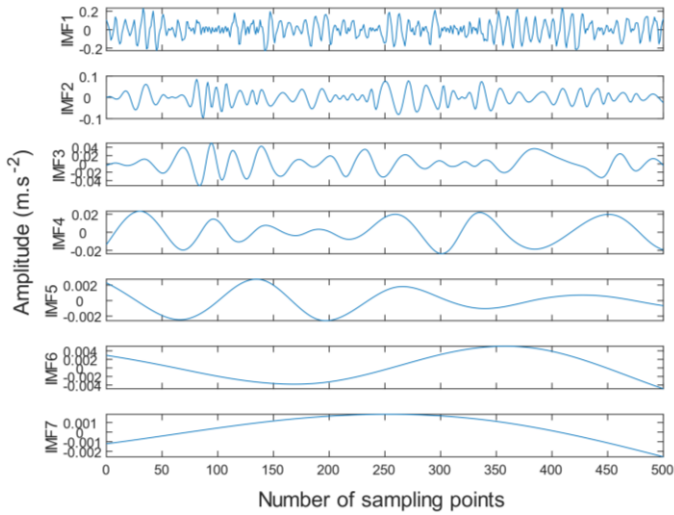
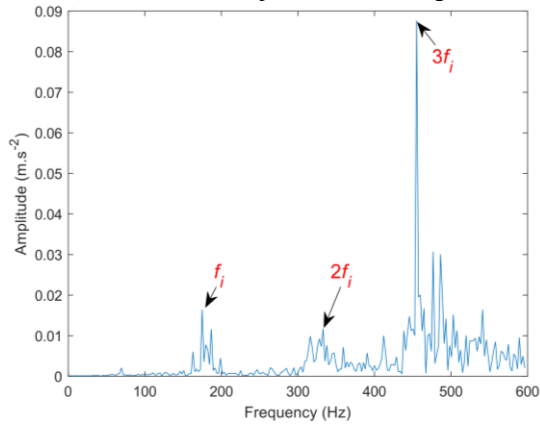


Fig. 11. Fault signal of bearing inner ring

The fault signals are processed using non-extension EMD, mirror extension EMD, and SIEMD. The components after decomposition are as follows.

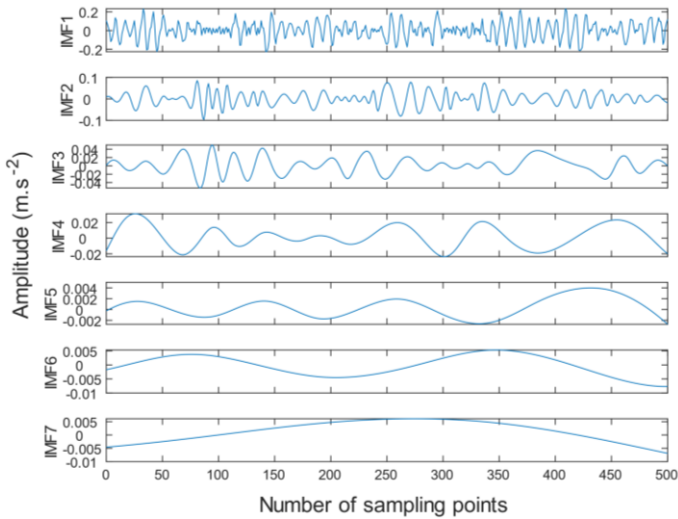


a) The EMD decomposition of fault signals

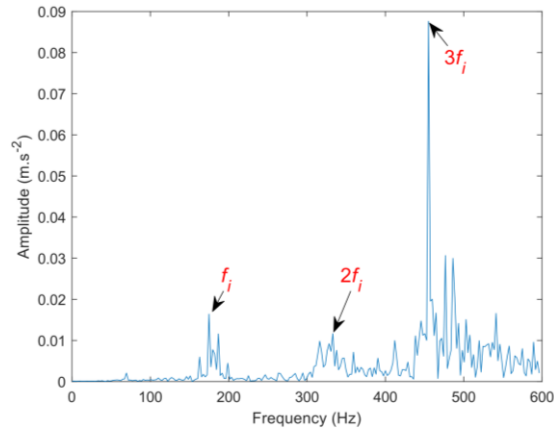


b) Spectrum corresponding to IMF<sub>1</sub> component

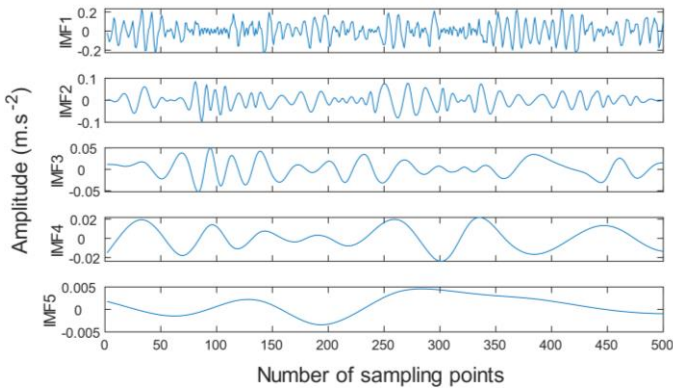
**Fig. 12.** The EMD decomposition



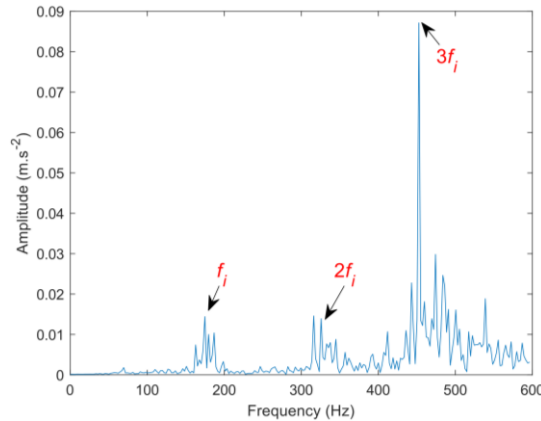
a) Mirror extension EMD decomposition of fault signal



b) Spectrum corresponding to IMF<sub>1</sub> component  
**Fig. 13.** Mirror extension EMD decomposition



a) The EMD decomposition of fault signal by SIEMD



b) Spectrum corresponding to IMF<sub>1</sub> component  
**Fig. 14.** The SIEMD decomposition

Compared to Figs. 12-14, the traditional EMD and mirror extended EMD decomposed the signal into seven components. Whereas the SIEMD method decomposed the signal into only five IMF components. Excessive components will reduce the signal fault extraction rate and may cause information redundancy and dimension disaster. Comparing the spectrum, it can be seen that the SIEMD method is more prominent at the second harmonic frequency, which is convenient for

accurately judging the fault type.

The data in Table 3 are the correlation coefficients between the first four components of the bearing inner ring fault signal and EMD, mirror EMD, and SIEMD and the fault signal. According to the data in Table 3, the similarity between IMF<sub>1</sub> component and fault signal is the highest, while the similarity between component IMF<sub>4</sub> and fault signal is the lowest, indicating that the similarity between each component and fault signal is decreasing, that is, the first component obtained has more fault information and has the highest correlation with fault signal. Compared with EMD [22], mirror EMD [16] and SIEMD, the similarity between the component obtained by the SIEMD method and the fault signal is the highest, reaching 92.03 %, which has greater advantages than the other two methods. If the correlation coefficient between the two is large, it is judged to be an effective IMF component. If the correlation coefficient between the two is small, it is judged to be a false component. The double fault frequency at Fig. 14(b) is more prominent than other methods. Therefore, compared with the mirror extension method, SIEMD can weaken the influence of the endpoint effect to a greater extent and extract the signal fault signal faster.

**Table 3.** Evaluation index values of the three methods

	$\rho_1(y(t), IMF_1(t))$	$\rho_2(y(t), IMF_2(t))$	$\rho_3(y(t), IMF_3(t))$	$\rho_4(y(t), IMF_4(t))$
SIEMD	0.9203	0.3327	0.1038	0.0449
Mirror extension	0.9198	0.3356	0.1002	0.0421
Non-extension	0.9200	0.3338	0.1034	0.0402

## 7. Conclusions

Here, the SIEMD method is proposed to suppress the end effect of the EMD. Considering the slope of signal extremum and motion energy, this method uses the least squares-polynomial fitting to extend the waveform of fault signal.

Compared with the traditional EMD [22] and mirror EMD [16], the proposed SIEMD decomposition method extracts less IMF components, higher correlation coefficient, and smaller relative error. It is beneficial for the extraction of fault feature information.

The SIEMD method overcomes the shortcomings of the original signal waveform and can effectively suppress the endpoint effect generated by the EMD. Therefore, the decomposition accuracy of this method is superior to that of the EMD.

The subsequent work will study the influence of signal waveform on signal decomposition and the significance of signal energy to signal decomposition, and propose a new decomposition method on this basis.

## Acknowledgements

The authors would like to acknowledge the anonymous reviewers for their valuable and constructive comments. This study was supported by the National Natural Science Foundation Project (Grant numbers 51966018 and 51466015) and the Key Research & Development Program of Xinjiang (Grant number 2022B01003).

## Data availability

The datasets generated during and/or analyzed during the current study are available from the corresponding author on reasonable request.

## Author contributions

Yuanjun Dai: visualization, supervision, validation. Weiqiang Huang: writing-original draft preparation, software, conceptualization. Kunju Shi: writing-review and editing, visualization.

## Conflict of interest

The authors declare that they have no conflict of interest.

## References

- [1] Y. Cheng, B. Chen, G. Mei, Z. Wang, and W. Zhang, "A novel blind deconvolution method and its application to fault identification," *Journal of Sound and Vibration*, Vol. 460, p. 114900, Nov. 2019, <https://doi.org/10.1016/j.jsv.2019.114900>
- [2] M. Demetgul, K. Yildiz, S. Taskin, I. N. Tansel, and O. Yazicioglu, "Fault diagnosis on material handling system using feature selection and data mining techniques," *Measurement*, Vol. 55, pp. 15–24, Sep. 2014, <https://doi.org/10.1016/j.measurement.2014.04.037>
- [3] X. Ye, Y. Hu, J. Shen, C. Chen, and G. Zhai, "An adaptive optimized TVF-EMD based on a sparsity-impact measure index for bearing incipient fault diagnosis," *IEEE Transactions on Instrumentation and Measurement*, Vol. 70, pp. 1–11, 2021, <https://doi.org/10.1109/tim.2020.3044517>
- [4] C. Yin, Y. Wang, G. Ma, Y. Wang, Y. Sun, and Y. He, "Weak fault feature extraction of rolling bearings based on improved ensemble noise-reconstructed EMD and adaptive threshold denoising," *Mechanical Systems and Signal Processing*, Vol. 171, p. 108834, May 2022, <https://doi.org/10.1016/j.ymsp.2022.108834>
- [5] A. Mejia-Barron, M. Valtierra-Rodriguez, D. Granados-Lieberman, J. C. Olivares-Galvan, and R. Escarela-Perez, "The application of EMD-based methods for diagnosis of winding faults in a transformer using transient and steady state currents," *Measurement*, Vol. 117, pp. 371–379, Mar. 2018, <https://doi.org/10.1016/j.measurement.2017.12.003>
- [6] O. Abedinia, M. Lotfi, M. Bagheri, B. Sobhani, M. Shafie-Khah, and J. P. S. Catalao, "Improved EMD-based complex prediction model for wind power forecasting," *IEEE Transactions on Sustainable Energy*, Vol. 11, No. 4, pp. 2790–2802, Oct. 2020, <https://doi.org/10.1109/tste.2020.2976038>
- [7] N. Bokde, A. Feijóo, D. Villanueva, and K. Kulat, "A review on hybrid empirical mode decomposition models for wind speed and wind power prediction," *Energies*, Vol. 12, No. 2, p. 254, Jan. 2019, <https://doi.org/10.3390/en12020254>
- [8] C. Guo, Y. Chen, J. Yuan, Y. Zhu, Q. Cheng, and X. Wang, "Biomedical photoacoustic imaging optimization with deconvolution and EMD reconstruction," *Applied Sciences*, Vol. 8, No. 11, p. 2113, Nov. 2018, <https://doi.org/10.3390/app8112113>
- [9] T. Hu, Z. Li, C. Zeng, G. Li, and H. Zhang, "Applications of EMD to analyses of high-frequency beachface responses to Storm Bebinca in the Qing'an Bay, Guangdong Province, China," *Acta Oceanologica Sinica*, Vol. 41, No. 5, pp. 147–162, May 2022, <https://doi.org/10.1007/s13131-021-1948-2>
- [10] M. R. Hossain, M. T. Ismail, and S. A. B. A. Karim, "Improving stock price prediction using combining forecasts methods," *IEEE Access*, Vol. 9, pp. 132319–132328, 2021, <https://doi.org/10.1109/access.2021.3114809>
- [11] J. Yang, G. Shi, T. Zhou, and F. Gao, "Waveform extension method based on similarity sequential detection for the end effects reduction of EMD," *Journal of Vibration and Shock*, Vol. 37, pp. 121–125, 2018, <https://doi.org/10.13465/j.cnki.jvs.2018.18.017>
- [12] L. Wang and Z. Liu, "An improved local characteristic-scale decomposition to restrict end effects, mode mixing and its application to extract incipient bearing fault signal," *Mechanical Systems and Signal Processing*, Vol. 156, p. 107657, Jul. 2021, <https://doi.org/10.1016/j.ymsp.2021.107657>
- [13] W. Zhou, Z. Feng, Y. F. Xu, X. Wang, and H. Lv, "Empirical Fourier decomposition: An accurate signal decomposition method for nonlinear and non-stationary time series analysis," *Mechanical Systems and Signal Processing*, Vol. 163, p. 108155, Jan. 2022, <https://doi.org/10.1016/j.ymsp.2021.108155>
- [14] D. Cao, J. Kang, J. Zhao, and X. Zhang, "Research on the comparison with methods of restraining ending effect of EMD and its application in fault diagnosis," *Journal of Mechanical Transmission*, Vol. 37, No. 3, pp. 83–87, 2013, <https://doi.org/10.16578/j.issn.1004.2539.2013.03.009>
- [15] Z. Zhang and W. Cui, "Method for restraining the end-effect of local characteristic-scale decomposition based on the mixed interpolation and polynomial correction," *Journal of Vibration and Shock*, Vol. 37, No. 22, pp. 181–186, 2018, <https://doi.org/10.13465/j.cnki.jvs.2018.22.027>
- [16] X. Zhang, Y. Huo, and D. Wan, "Improved EMD based on piecewise cubic hermite interpolation and mirror extension," *Chinese Journal of Electronics*, Vol. 29, No. 5, pp. 899–905, Sep. 2020, <https://doi.org/10.1049/cje.2020.08.005>

- [17] J. Chen, Z. Dong, H. Li, X. Yang, and X. Zhang, "LMD endpoint effect suppression of sampling point slope matching data sequence extension and deformation information extraction," *Geomatics and Information Science of Wuhan University*, 2021.
- [18] N. Marchon, G. Naik, and R. Pai, "Monitoring of fetal heart rate using sharp transition FIR filter," *Biomedical Signal Processing and Control*, Vol. 44, pp. 191–199, Jul. 2018, <https://doi.org/10.1016/j.bspc.2018.04.017>
- [19] T. Xu, C. Lu, H. Wang, and X. Han, "Failure rate prediction method based on relevance vector EMD and GMDH reconstruction," *Journal of Vibration, Measurement and Diagnosis*, Vol. 38, No. 6, pp. 1275–1285, 2018, <https://doi.org/10.16450/j.cnki.issn.1004-6801.2018.06.030>
- [20] B. Xu, F. Zhou, Y. Ma, B. Yan, and H. Li, "Feature extraction of rolling bearing's slight fault of SPPCS CEEMD based on HLS-SVDR," *Journal of Vibration, Measurement and Diagnosis*, Vol. 39, No. 1, pp. 136–146, 2019, <https://doi.org/10.16450/j.cnki.issn.1004-6801.2019.01.021>
- [21] A. Kumar Shakya and S. Singh, "Design of novel Penta Core PCF SPR RI sensor based on fusion of IMD and EMD techniques for analysis of water and transformer oil," *Measurement*, Vol. 188, p. 110513, Jan. 2022, <https://doi.org/10.1016/j.measurement.2021.110513>
- [22] Y. Lei, J. Lin, Z. He, and M. J. Zuo, "A review on empirical mode decomposition in fault diagnosis of rotating machinery," *Mechanical Systems and Signal Processing*, Vol. 35, No. 1-2, pp. 108–126, Feb. 2013, <https://doi.org/10.1016/j.ymsp.2012.09.015>
- [23] W. Su, S. Zhang, and L. Liu, "Suppression of end effect of pole-symmetric modal decomposition based on improved extremum wave continuation," *Transactions of China Electrotechnical Society*, pp. 294–301, 2020, <https://doi.org/10.19595/j.cnki.1000-6753.tces.180062>
- [24] C. Grenat, S. Baguet, C.-H. Lamarque, and R. Dufour, "A multi-parametric recursive continuation method for nonlinear dynamical systems," *Mechanical Systems and Signal Processing*, Vol. 127, pp. 276–289, Jul. 2019, <https://doi.org/10.1016/j.ymsp.2019.03.011>
- [25] K. Zhang, J. Cheng, and Y. Yang, "Processing method for end effects of local mean decomposition based on self-adaptive waveform matching extending," *China Mechanical Engineering*, Vol. 21, No. 4, pp. 457–462, 2010.
- [26] M. Sheikh-Hosseini, M. Hasheminejad, and F. Rahdari, "Linear precoder design for peak-to-average power ratio reduction of generalized frequency division multiplexing signal using gradient descent methods," *Transactions on Emerging Telecommunications Technologies*, Vol. 34, No. 2, Feb. 2023, <https://doi.org/10.1002/ett.4698>
- [27] M. Liu, H. Fan, Y. Zhang, Z. Li, and W. Yang, "Adaptive multi-scale method for the non-linear dynamic feature extraction of mechanical vibration signals," *Journal of Vibration and Shock*, Vol. 39, No. 14, pp. 224–232, 2020, <https://doi.org/10.13465/j.cnki.jvs.2020.14.031>
- [28] J. Zhong, T. Chen, F. Peng, X. Bi, and Z. Chen, "Direction of arrival estimation based on slope fitting of wideband array signal in fractional Fourier transform domain," *IET Radar, Sonar and Navigation*, Vol. 17, No. 3, pp. 422–434, Mar. 2023, <https://doi.org/10.1049/rsn2.12350>
- [29] L. Liu, X. Zhang, and Y. Lei, "Data-driven identification of structural damage under unknown seismic excitations using the energy integrals of strain signals transformed from transmissibility functions," *Journal of Sound and Vibration*, Vol. 546, p. 117490, Mar. 2023, <https://doi.org/10.1016/j.jvs.2022.117490>
- [30] J. Shi, H. Shen, and Z. Ding, "Quantitative analysis of broken rotor bars in cage motor based on energy characteristics of vibration signals," *Computational Intelligence and Neuroscience*, Vol. 2022, pp. 1–12, Jun. 2022, <https://doi.org/10.1155/2022/9312876>



**Yuanjun Dai**, Professor, doctoral supervisor. He is mainly engaged in fluid mechanical noise control technology and fluid-solid coupling control technology. In the past five years, it has presided over and mainly completed 24 scientific research projects, published 58 papers in international and domestic important conferences and core journals, and 22 papers were retrieved by SCI and EI. He is also a reviewer of the National Natural Science Foundation of China, a reviewer of the Inner Mongolia Natural Science Foundation, a member of the Standing Committee of the Modern Manufacturing Engineering Expert Committee, and a reviewer of magazines such as JMES.





**Weiqiang Huang** received his bachelor's degree from Nanjing Institute of Engineering in 2017. He is currently a graduate student of Shanghai Dianji University. His research direction is mechanical fault diagnosis.



**Kunju Shi** received the B.E. degree in Measurement and Control Technology from North China University of Science and Technology, Tangshan, China, in 2009, the M.S. degree in Machine Design Manufacture and Automate from Lanzhou University of Technology, Lanzhou, China, in 2013, and the Ph.D. degree in Mechatronic Engineering from the Shanghai University, Shanghai, China, in 2016. Since 2019, he has been a lecturer with Machinery College, Shanghai Dianji University.